Tellus (1999), 51A-B, 123–146
Printed in UK – all rights reserved

TELLUS
ISSN 0280–6495
ISSN 0280–6509

On the background photochemistry of tropospheric ozone

By PAUL J. CRUTZEN*, MARK G. LAWRENCE and ULRICH PÖSCHL, *Max-Planck-Institute for Chemistry, PF 3060, 55020 Mainz, Germany*

(Manuscript received 4 September 1998; in final form 21 September 1998)

ABSTRACT

We present a largely tutorial overview of the main processes that influence the photochemistry of the background troposphere. This is mostly driven by the photolysis of ozone by solar ultraviolet radiation of wavelengths shorter than about 340 nm, resulting in production of excited $O(^1D)$ atoms, whose reaction with water vapor produces OH radicals. In the background atmosphere the OH radicals mostly react with CO, and with CH_4 and some of its oxidation products, which in turn are oxidized by OH. Depending on the availability of NO_x catalysts, ozone may be produced or destroyed in amounts that are much greater than the downward flux of ozone from the stratosphere to the troposphere. Using the 3D chemical-transport model MATCH, global distributions and budget analyses are presented for tropospheric O_3, CH_4, CO, and the "odd hydrogen" compounds OH, HO_2 and H_2O_2. We show that OH is present in maximum concentrations in the tropics, and that most of the chemical breakdown of CO and CH_4 also occurs in equatorial regions. We also split the troposphere into continental and marine regions, and show that there is a tremendous difference in photochemical O_3 and OH production for these regions, much larger than the difference between the northern hemisphere and southern hemisphere. Finally, we show the results from a numerical simulation in which we reduced the amount of ozone in the model stratosphere by a factor of 10 (which in turn reduced the flux of O_3 into the troposphere by about the same factor). Nevertheless, for summer conditions, model calculated O_3 mixing ratios below 5 km in the mid to high latitudes were about 70–90% as high as those calculated with the full downward flux of ozone from the stratosphere. This indicates that, at least under these conditions, O_3 concentrations in the lower troposphere are largely controlled by in situ photochemistry, with only a secondary influence from stratospheric influx.

1. Introduction

The chemistry of the atmosphere involves many compounds present in the parts per million range or even much less than that. One of the most important photochemically active gases is O_3. About 90% of this gas, which shields life on earth from hazardous ultraviolet radiation, is present in the stratosphere. There is much to discuss about stratospheric ozone, especially how it has been so strongly diminished by human activities near the poles during winter-spring, but in this article we will focus on the important chemical rôle of the relatively small amount of ozone which is located in the troposphere.

Until about 25 years ago, it was generally believed that, except near some urban regions, all ozone in the troposphere was initially formed in the stratosphere, its downward flux to the troposphere being balanced by loss at the earth's surface (Fabian and Junge, 1970). Within the troposphere ozone was considered to be inert. We know now that this simple concept was far from correct. In fact, the chemistry of the troposphere is largely driven by solar ultraviolet radiation of wavelengths shorter than about 340 nm whose photons are able to dissociate O_3 into O_2 and electronically excited $O(^1D)$ atoms (Michelsen et al., 1994)

R1 $\quad O_3 + h\nu \rightarrow O(^1D) + O_2$ ($\lambda < 340$ nm).

* Corresponding author.

While most of the excited O atoms are collisionally deactivated to ground state O atoms which again form O_3 via

R2 $O + O_2 + M \rightarrow O_3 + M$,

the remaining $O(^1D)$ atoms have enough energy to react with water vapour to produce OH radicals

R3 $O(^1D) + H_2O \rightarrow 2OH$.

The hydroxyl radicals, the "detergents" of the atmosphere, react with most gases that are emitted to the atmosphere by natural processes or human activities. Despite their very low relative abundance in the troposphere, globally averaged there are only about 4 OH molecules per 10^{14} air molecules at the surface (see below), it is this highly reactive radical, and not the almost 10^{13} times more abundant O_2, which initiates almost all oxidation processes in the atmosphere. The discovery of the oxidative rôle of OH in the atmosphere was thus a milestone in our understanding of the chemistry of the atmosphere (Levy, 1971). Prior to 1971 it was simply not known how the many gases which are emitted into the atmosphere are again removed. Not surprising, earlier published budgets of atmospheric trace gases were grossly incorrect. It is interesting to note: on the one hand the so-called UV-B radiation with wavelengths below 340 nm can be harmful to the biosphere, while on the other hand it is of great benefit by keeping the atmosphere "clean" through the production of OH radicals, the "detergents of the atmosphere," via reactions R1 and R3.

The atmospheric lifetimes for many gases are largely determined by the efficiency with which they react with OH. Methylchloroform (CH_3CCl_3) has been especially useful for estimating the average concentrations of OH in the troposphere. It has solely been produced in known amounts by the chemical industry and is largely removed by reaction with OH. Consequently, with knowledge about its global distribution and rate of change over time, CH_3CCl_3 can be used to estimate the average concentration of OH in the troposphere. This is close to 10^6 molecules/cm^3, corresponding to the surface volume mixing ratio of 4×10^{-14} mentioned before (e.g., Krol et al., 1998; Prinn et al., 1995). Direct measurements of OH radicals in the atmosphere, although important for testing photochemical theory, can not provide us with this number, too variable are the concentrations of OH, and too elaborate and expensive the techniques to measure them. The atmospheric lifetime of CH_3CCl_3 is about 4.6 years (Prinn et al., 1995). Because its production was stopped at the beginning of 1996, a substantial reduction of its abundance in the atmosphere has been clearly observed (Montzka et al., 1996). CH_4 reacts more slowly with OH than CH_3CCl_3; its atmospheric lifetime is about 8 years. CH_4 thus has a volume mixing ratio distribution with relatively little variability in space and time, and only about 5% higher concentration in the northern hemisphere, into which it is mostly released, than in the southern hemisphere (Dlugokencky et al., 1994; Fung et al., 1991). Other hydrocarbons react more rapidly with OH, which is reflected in shorter atmospheric lifetimes, larger spatial and temporal variability, and greater interhemispheric gradients. The highly reactive compound isoprene (C_5H_8) has in fact such a short atmospheric lifetime, a few hours, that it can only be detected in significant quantities within some 100 km downwind from the forest regions in which it is produced. Among the gases that are removed by reaction with OH, there are also several that are entirely manmade: besides CH_3CCl_3, the so-called HCFC and the HFC gases, the replacement products for the fully halogenated CFC gases ($CFCl_3$ and CF_2Cl_2). Due to their reaction with OH the atmospheric residence times of the HCFCs and HFCs are much shorter than those of the CFCs and their danger for the ozone layer much smaller than that caused by the CFCs, which are only broken down by photodissociation in the stratosphere.

The main gases with which OH reacts in the background atmosphere are CO and CH_4, and the CH_4-oxidation products CH_3O_2H and CH_2O. Although reactions with more reactive hydrocarbons, especially those of natural origin such as isoprene (C_5H_8), can indirectly play a significant rôle also in background chemistry through the formation of carbon monoxide, and through providing a sink for OH concentrations near forested regions, especially in the tropics (Wang et al., 1998; Houweling et al., 1998), we will restrict our discussion in this study to the chemical reactions taking place in the background O_3–NO_x–HO_x–CH_4–CO system. Contrary to the general thinking until about 25 years ago and following many analyses since Crutzen (1973), we will show that much more ozone is formed and destroyed by

photochemical reactions in the troposphere than the amounts that are transported down from the stratosphere. That does not mean, however, that the stratospheric O_3 supply to the troposphere only plays a minor rôle. Without the influx of stratospheric ozone, tropospheric photochemistry would have to be initialized by much weaker primary sources of HO_x radicals than provided by reaction R3 (e.g., photolysis of carbonyls). However, following the supply of stratospheric ozone to the troposphere, autocatalytic chains of reactions are activated which can produce or destroy ozone, largely regulated by the availability of NO_x ($NO + NO_2$). In these chains, OH and the related reactive hydrogen oxide compounds, HO_2 and H_2O_2, are often recycled as well.

In this study, we will present an analysis of the most important terms in the chemical budgets of tropospheric ozone and hydrogen oxides, based on the results obtained with the global three-dimensional model MATCH, which considers the background chemistry of the troposphere, involving reactions R1 and R3, and the CO and CH_4 oxidation reaction sequences, as discussed in the next section.

2. Background photochemistry of the troposphere: CH_4 and CO oxidation

Following OH production via reactions R1 and R3, which also provide a sink for ozone, the OH radical can initiate reactions leading to the formation or destruction of ozone, depending on the concentrations of reactive NO and NO_2 (Crutzen, 1973). Carbon monoxide is oxidized by OH

R4 $\quad CO + OH(+O_2) \rightarrow CO_2 + HO_2$

The HO_2 radicals can next react with NO

R5 $\quad HO_2 + NO \rightarrow OH + NO_2$,

rapidly followed by NO_2 photolysis and O_3 formation.

R6 $\quad NO_2 + h\nu \rightarrow NO + O$

R7 $\quad O + O_2 + M \rightarrow O_3 + M$

with the overall net result

C1: $\quad CO + 2O_2 \rightarrow CO_2 + O_3$.

The HO_2 radicals can, however, also react with O_3

R8 $\quad HO_2 + O_3 \rightarrow OH + 2O_2$

The net result of reactions R4 + R8 is the destruction of one ozone molecule:

C2: $\quad CO + O_3 \rightarrow CO_2 + O_2$

In the troposphere most HO_2 is formed by reaction R4; a minority, however, also by the reaction

R9 $\quad OH + O_3 \rightarrow HO_2 + O_2$

In that case reactions R9 + R5 + R6 + R7 constitute a do-nothing cycle, while the reaction pair R9 + R8 leads to the loss of 2 ozone molecules.

Reactions with peroxy radicals, such as reaction R5, are not the main source of NO_2 in the atmosphere. Most NO_2 is formed by

R10 $\quad NO + O_3 \rightarrow NO_2 + O_2$

Reaction sequence R10 + R6 + R7 performs a null cycle without any net ozone production. Reaction R10 does, however, shift the balance of NO to NO_2, making less NO available for the production of ozone. Note that in the reaction sequences C1 and C2 OH, HO_2, NO and NO_2 act as catalysts. Such reaction sequences involving several catalysts are characteristic of atmospheric photochemistry.

Further reactions with HO_2 or CH_3O_2 can lead to the formation of H_2O_2 and CH_3O_2H:

R11 $\quad HO_2 + HO_2 \rightarrow H_2O_2 + O_2$

R12 $\quad HO_2 + CH_3O_2 \rightarrow CH_3O_2H + O_2$

Which of the CO oxidation branches C1 or C2 is more important depends strongly on the atmospheric concentrations of nitrogen oxides, NO_x ($NO + NO_2$). These come from a variety of natural and anthropogenic sources and have short atmospheric lifetimes of only a few days, due to conversion to nitric acid (HNO_3) either via the reaction $NO_2 + OH + M \rightarrow HNO_3 + M$ during daytime or via the heterogeneous reaction $N_2O_5 + H_2O \rightarrow 2HNO_3$ on particle surfaces during night. One finds highly variable concentrations of nitrogen oxides in space and time. The regions in the world where net ozone production occurs in the troposphere are those containing enough NO. The most important anthropogenic sources of NO include the burning of fossil fuels, producing approximately 20–25 million tons of N per year (Benkovitz et al., 1996; Hameed and Dignon, 1991), and biomass burning from which approximately 2–13 million tons of N are annually emitted to the atmosphere largely during the dry season in the tropics and subtropics (Crutzen and

Andreae, 1990; Dignon and Penner, 1991, Hao and Liu, 1994). Comparing this quantity with the estimated natural emissions from soils of 3–8 million tons N per year (Yienger and Levy, 1995), which are also in part anthropogenic (via the use of N fertilizers in agriculture), and from lightning (1–20 million ton N/year; Lawrence et al., 1995, Price et al., 1997), one recognizes that the anthropogenic NO emissions are probably higher than the natural ones.

The CO oxidation sequence, discussed above, is the simplest example of how ozone can be formed in the troposphere; the methane oxidation sequence is somewhat more complex (see below), while the oxidation of the higher hydrocarbons can involve up to thousands of reactions. The final result is, however, similar: if nitrogen oxides are present in significant quantities together with CO, CH_4, or more reactive hydrocarbons, ozone will be formed; otherwise ozone destruction can occur. During summertime high pressure fair weather conditions, which combine plenty of solar UV radiation with meteorologically stable conditions during which pollutants are trapped in the lower troposphere, high concentrations of ozone can be produced over large areas, leading to so-called photochemical smog.

The oxidation sequences of methane, as summarized in Fig. 1, strongly affect the atmospheric budgets of hydroxyl and ozone (Crutzen, 1973), to be quantified in the next section. Again, as for CO, nitric oxide plays an important catalytic rôle in determining the oxidation pathways and products in the CH_4 oxidation sequence. In NO-rich environments, following the reaction of OH with CH_4, formation of ozone and formaldehyde (CH_2O) occurs within minutes with OH, HO_2, NO and NO_2 serving as catalysts:

R13 $CH_4 + OH(+O2) \rightarrow CH_3O_2 + H_2O$

R14 $CH_3O_2 + NO \rightarrow CH_3O + NO_2$

R15 $CH_3O + O_2 \rightarrow CH_2O + HO_2$

R5 $HO_2 + NO \rightarrow OH + NO_2$

R6 (2×) $NO_2 + v \rightarrow NO + O$ ($\lambda < 400$ nm)

R7 (2×) $O + O_2 + M \rightarrow O_3 + M$

net C3: $CH_4 + 4O_2 \rightarrow CH_2O + H_2O + 2O_3$.

In NO-poor environments, CH_4 is predominantly oxidized to CH_2O without O_3 formation

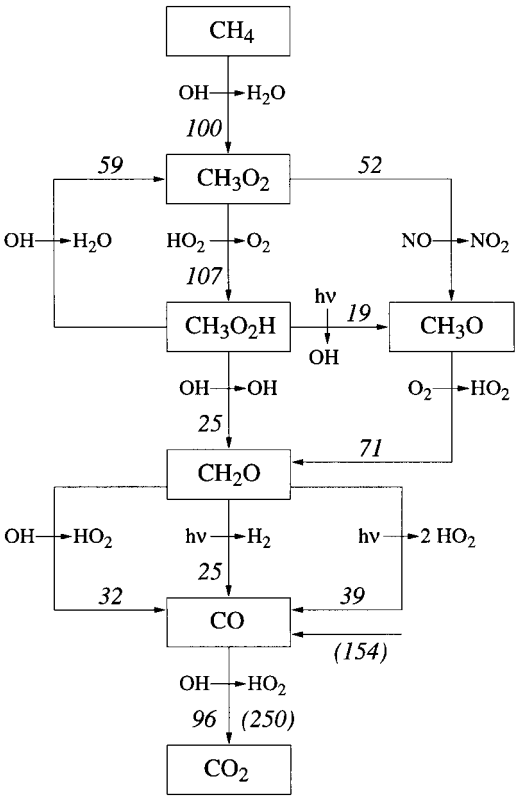

Fig. 1. CH_4 oxidation pathways. Reaction rates for the global troposphere are scaled to the primary step $CH_4 + OH$ (100, corresponding to a globally averaged flux of 1.06×10^{11} molecules $cm^{-2}\,s^{-1}$); minor pathways (<5) are neglected.

by either of the following two pathways

R13 $CH_4 + OH(+O_2) \rightarrow CH_3O_2 + H_2O$

R12 $CH_3O_2 + HO_2 \rightarrow CH_3O_2H + O_2$

R16 $CH_3O_2H + h\nu \rightarrow$
$CH_3O + OH$ ($\lambda < 340$ nm)

R15 $CH_3O + O_2 \rightarrow CH_2O + HO_2$

net C4: $CH_4 + O_2 \rightarrow CH_2O + H_2O$

or

R13 $CH_4 + OH(+O_2) \rightarrow CH_3O_2 + H_2O$

R12 $CH_3O_2 + HO_2 \rightarrow CH_3O_2H + O_2$

R17a $CH_3O_2H + OH \rightarrow CH_2O + H_2O + OH$

net C5: $CH_4 + OH + HO_2 \rightarrow CH_2O + 2H_2O$

A subcycle; the catalytic pair of reactions

R12 $CH_3O_2 + HO_2 \rightarrow CH_3O_2H + O_2$

R17b $CH_3O_2H + OH \rightarrow CH_3O_2 + H_2O$

net C6: $OH + HO_2 \rightarrow H_2O + O_2$

is an important sink for HO_x ($OH + HO_2$) radicals. The oxidation pathways of methane in NO-poor environments are, therefore, far more complex than in NO-rich environments. It is, however, clear that HO_x radicals tend to be lost.

Three reaction pathways lead to the further oxidation of CH_2O to CO:

R18a $CH_2O + h\nu \rightarrow H + CHO$ ($\lambda \leqslant 350$ nm)

R19 $H + O_2 + M \rightarrow HO_2 + M$

R20 $CHO + O_2 \rightarrow CO + HO_2$

net C7a: $CH_2O + 2O_2 \rightarrow CO + 2HO_2$

or

R21 $CH_2O + OH \rightarrow CHO + H_2O$

R20 $CHO + O_2 \rightarrow CO + HO_2$

net C7b: $CH_2O + OH + O_2 \rightarrow CO + H_2O + HO_2$

or directly via

R18b $CH_2O + h\nu \rightarrow CO + H_2$ ($\lambda \leqslant 350$ nm)

The HO_2 radicals formed in reactions R4, R9, R15 and reaction sequences C7a and C7b can react further via R5, R8, R11 or R12, leading to formation or destruction of O_3, or production of hydroperoxides, depending on chemical conditions, in particular ambient concentrations of NO and O_3.

3. Model results

An important way of trying to gain an understanding of how the photochemistry of the atmosphere works on a large scale is through the development of global numerical models of atmospheric transport and chemistry. Although it has been over a decade since the development of the first three-dimensional global chemistry-transport models (CTMs) (Levy et al, 1985; Crutzen and Zimmermann, 1991), and significant progress has been made in that time, they can still be considered to be in their early stages of development. The most detailed of these models uses grids which are 100×100 km in horizontal dimensions, and about 1 km in the vertical. However, computations at such high resolutions can take literally weeks to complete, so that it is often preferred to use a lower resolution, such as 1000×1000 km in the horizontal. Even at the highest resolution, many processes which affect tropospheric chemistry, such as convective storms, cannot be resolved and must therefore be parameterized; this problem is only compounded at lower resolutions. Nevertheless, global models are useful tools for gaining a basic understanding of the processes which are most important in tropospheric chemistry.

In this section, we consider the results from a newly-developed model known as MATCH (Model of Atmospheric Transport and CHemistry; Rasch et al.,1997, Mahowald et al., 1997, Lawrence, 1996). The transport for these simulations is based on the meteorological reanalysis from the National Centers for Environmental Prediction (with 6-hourly T, P, U, and V based on global observations; Kalnay et al., 1996). For advective transport, MATCH employs the new SPITFIRE scheme (Rasch and Lawrence, 1998). MATCH also includes parameterizations for vertical diffusion (Holtslag and Boville, 1993), convective cloud transport, using the same Zhang/McFarlane/Hack scheme that is employed in the NCAR CCM3 (Zhang and McFarlane, 1995; Hack, 1994), and non-convective cloud transport via gravitational sedimentation (Lawrence and Crutzen, 1998). The model is run at an intermediate resolution (T21, approx. 500×500 km) for this study.

The photochemistry part of the model handles sources, transformations, and sinks of key trace gases (O_3, HO_x, NO_y, CO, CH_4, and the CH_4 oxidation products). The sources included for NO_x are (in units of Tg(N)/yr) from: industry (21.3; Benkovitz et al., 1996), biomass burning (8.5; Hao and Liu, 1994), soils (5.5; Yienger and Levy, 1995), lightning (1.7; Lawrence et al., 1995; Price and Rind, 1992), and aircraft (0.4; Baughcum et al., 1987), all in agreement with the ranges indicated earlier. Carbon monoxide has important direct sources (here for MATCH in units of Tg(CO)/yr) from fossil fuel combustion (500; Olivier et al., 1996), biomass burning (500; Hao and Liu, 1994) and the oceans (50; Bates et al., 1995). CO is also produced by the oxidation of non-methane

hydrocarbons (300; Guenther et al., 1995); this is parameterized as an explicit surface source in the model (with the same distribution as the non-methane hydrocarbon emissions, but scaled to 300 Tg(CO)/yr), whereas CO production by the CH_4 oxidation sequences is computed in detail (via R18b, C7a, and C7b). The stratosphere-troposphere exchange (STE) sources of O_3 and NO_y, as well as the surface sources of CH_4, are handled by prescribing the mixing ratios of these species in the stratosphere according to observations. For O_3, we use monthly mean data from the HALOE satellite, and prescribe O_3 at the observed mixing ratios for all model levels above the pressure level defined by $P(\text{hPa}) = 220 - 165\cos(\phi)$, where ϕ is the latitude). NO_y is then held constant relative to O_3, based on the ratios observed by Murphy et al. (1993). Finally, surface CH_4 is prescribed based on the study of Fung et al. (1991).

The photochemical transformations of trace gases are handled by specifying reaction rate coefficients, absorption cross sections and quantum yields according to DeMore et al. (1997). Reaction rates are updated each time step, based on temperature and pressure. Photolysis frequencies are also calculated at each time step with the on-line computational method by Landgraf and Crutzen (1998), which uses actinic fluxes based on model ozone and cloud distributions. The set of photochemical reactions is then integrated forward in time each model time step (30 minutes), using quasi-steady-state approximations for the short-lived compounds, and Euler forward or backward approximations for compounds with long and medium lifetimes, respectively.

Finally, the model considers the loss of various trace gases by a few important processes. Deposition at the earth's surface ("dry deposition") is computed using deposition velocities which are supplied on a global grid from the study of Ganzeveld and Lelieveld (1995). Scavenging by precipitation ("wet deposition") is computed based on the cloud water contents and precipitation fluxes from MATCH (Rasch and Kristjansson, 1998). The heterogeneous loss of N_2O_5 via reactions on aerosols and cloud droplets is also included (Dentener and Crutzen, 1993).

These computations together result in trace gas distributions on a global grid over the simulated period of time (in this case 16 months), which can be compared with observations.

The transformation rates influencing the most important trace gases can also be tracked, allowing derivations of global and regional "budgets" for the formation and destruction of each trace gas, as discussed below.

In this section, we will use the model results to consider the following important aspects of tropospheric photochemistry: (1) the global distribution of O_3 and comparison to observations; (2) the global OH distribution; (3) the budgets of CO, CH_4, the HO_x radicals and H_2O_2; (4) the budget of tropospheric O_3; (5) the influence of stratosphere/troposphere exchange (STE) on the O_3 distribution in the troposphere.

3.1. *O_3 distribution*

The annual and seasonal zonal mean O_3 distributions computed by MATCH are depicted in Figs. 2 and 3. The main features to notice are: the tendency for O_3 mixing ratios to increase with height, and the generally lower O_3 levels in the tropics. The first feature is due to influx from the stratosphere and some net ozone production in the upper troposphere, along with uptake of ozone at the surface. Interestingly, based on where the isolines dip down most steeply into the troposphere, it appears that the main region of influx of stratospheric O_3 is at the subtropical tropopause break (near 30° latitude), rather than being near the jet stream at higher latitudes (this point is discussed further in Subsection 3.4). The second main feature is due to strong convective overturning and the upwelling branch of the Hadley cell near the equator, which pumps surface air low in O_3, due to destruction by reactions R1 + R3, into the middle and upper troposphere, maintaining the lower values shown in Figs. 2 and 3.

Tropospheric O_3 also shows a considerable variability with longitude. This is shown in Figs. 4, 5, which depict the seasonal mean O_3 distributions at the model levels representing approximately 900 hPa and 500 hPa pressure levels. Near the middle of the planetary boundary layer (Fig. 4), O_3 mixing ratios are generally highest over continental regions, both in the northern and southern hemisphere. The difference is most pronounced in the summer in the northern hemisphere, when photochemical production is strongest, and in the austral spring, when biomass burning is predominant in the southern

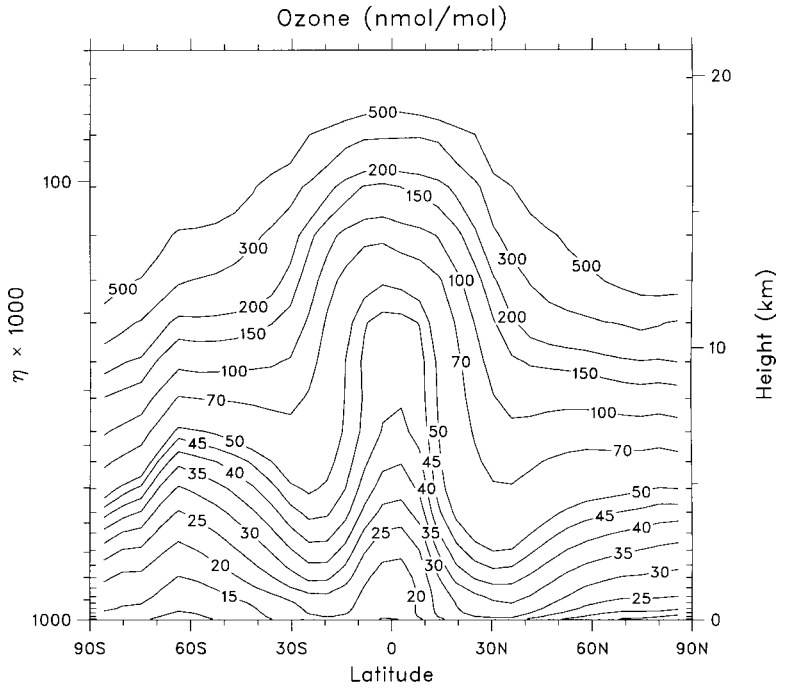

Fig. 2. Annual zonal mean O_3 distribution as computed by the 3-D chemistry transport model MATCH.

hemisphere. At 500 hPa, O_3 is somewhat more evenly distributed in longitude, due to its longer lifetime at this higher altitude. Some of the key features are the higher summer O_3 levels over North America compared to surrounding oceanic regions (showing that the influence of surface-level photochemical production can be fairly far-reaching), the biomass burning plume extending off of Africa in the latter half of the year, and the enhanced O_3 mixing ratios over South-Central Asia (the Himalayas), Greenland, and the Antarctic (these are due to the terrain-following coordinates in the model, so that the model levels at these three locations are at considerably higher altitudes than surrounding regions). A key feature to note in Fig. 5 is the band of elevated O_3 mixing ratios extending throughout the mid-latitudes in both hemispheres in the winter and spring, due to the strong STE O_3 influx through the subtropical tropopause break computed by this version of MATCH.

One of the most important tasks of global modelers is to test the quality of their models by making comparisons with observations. This helps to point out missing chemistry and/or deficiencies in the model. An extensive comparison of the MATCH results to observations is beyond the scope of this tutorial and is given for MATCH in other works (Lawrence, 1996; Lawrence and Crutzen, 1998; as well as several works already submitted or in preparation). However, we will give a sense of these comparisons here to provide a framework for the discussions which follow.

We begin by showing observed seasonal mean profiles (from Komhyr et al., 1989) versus MATCH output for four selected monitoring sites (Fig. 6). These sites were chosen to give a wide spread in latitude, and to represent regions which are relatively remote from the influence of non-methane hydrocarbons (NMHCs), which are not considered in the current version of MATCH. In these comparisons it can be seen that MATCH produces some of the main observed features, such as the tendency for O_3 mixing ratios to increase with altitude, the much higher tropopause height in the tropics than at higher latitudes, and the tendency for convective pumping to occasionally produce ozone minima in upper tropospheric

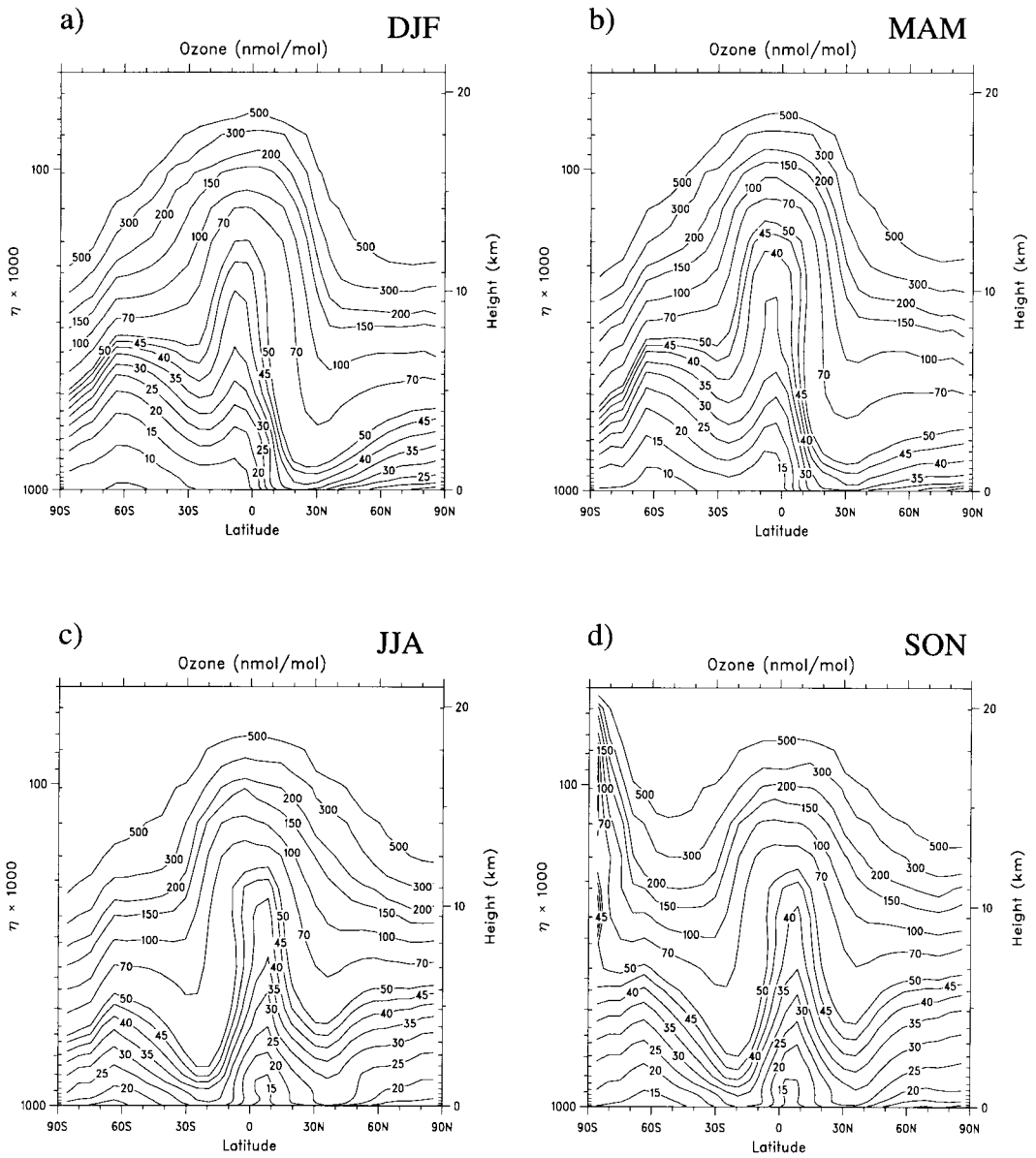

Fig. 3. Seasonal zonal mean O_3 distribution as computed by MATCH: (a) December–January–February (DJF), (b) March–April–May (MAM), (c) June–July–August (JJA), (d) September–October–November (SON). Note that the low stratospheric values at the South Pole during SON are due to the ozone hole, which is represented in the satellite data used to constrain the stratospheric O_3 values in the MATCH simulation.

mixing ratios relative to the mid-troposphere (Kley et al., 1996). However, this is not always the case, and it appears that in these runs the convective pumping might be too weak, particularly near Hilo, Hawaii.

In more extensive comparisons, we have found that in this version of MATCH, O_3 is generally underestimated at lower altitudes and overestimated at higher altitudes. We attribute this to two primary factors (which to an extent compens-

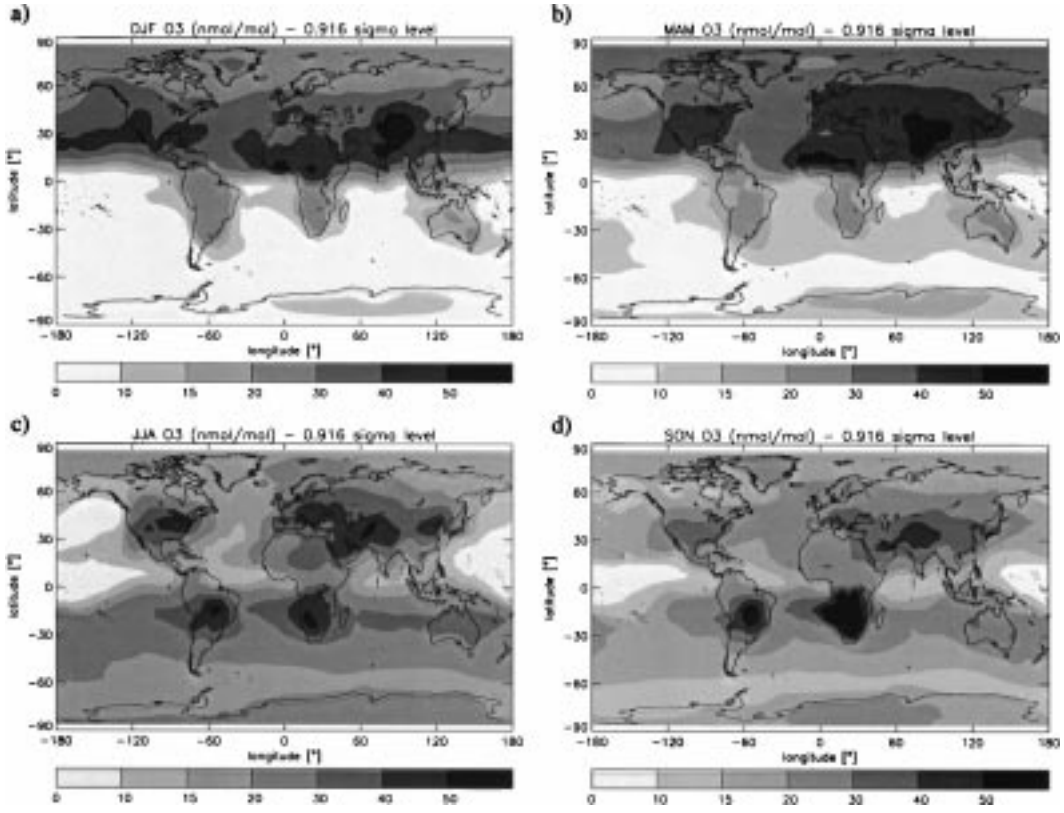

Fig. 4. The MATCH 0.916 sigma level seasonal mean O_3 distribution: (a) DJF, (b) MAM, (c) JJA, (d) SON. The data corresponds to an approximate pressure level of 900 hPa (the sigma level gives the pressure divided by the surface pressure, so that for a typical surface pressure of 1000 hPa, the pressure at 0.9 sigma is 900 hPa; thus high altitude regions such as the Himalayas show higher O_3 mixing ratios than surrounding regions).

ate each other, particularly in the upper troposphere). First, the STE downward flux of ozone in these runs is considerably higher than in many other studies (this is discussed in more detail in Subsection 3.4), leading to too high upper tropospheric ozone levels. Second, our NO_x levels in the current runs are much lower than in previous model versions (Lawrence, 1996), and on average significantly lower than observed NO_x mixing ratios, a problem which is common to many tropospheric chemistry models (Thakur et al., 1998). This likely results in underestimated O_3 production, and too low O_3 levels in the lower troposphere. We return to this particular issue in Subsection 3.4. For the following sections, it is important to keep these two peculiarities of these MATCH results in mind.

3.2. OH distribution

The critical rôle of OH in tropospheric chemistry was discussed in the previous sections. Since direct measurements of OH radicals are extremely difficult, and only performed on a very sparse basis to test photochemical theory, our best estimate of the global OH distribution comes from computations with global chemistry-transport models. In Figs. 7, 8, we show the annual and seasonal zonal mean OH concentrations as computed by the MATCH model described above. The most striking feature of these figures is the strong maximum near the surface in tropical regions. This is caused by maximum penetration of $O(^1D)$ producing ultraviolet radiation (reaction R1) due to a minimum in the ozone column, and

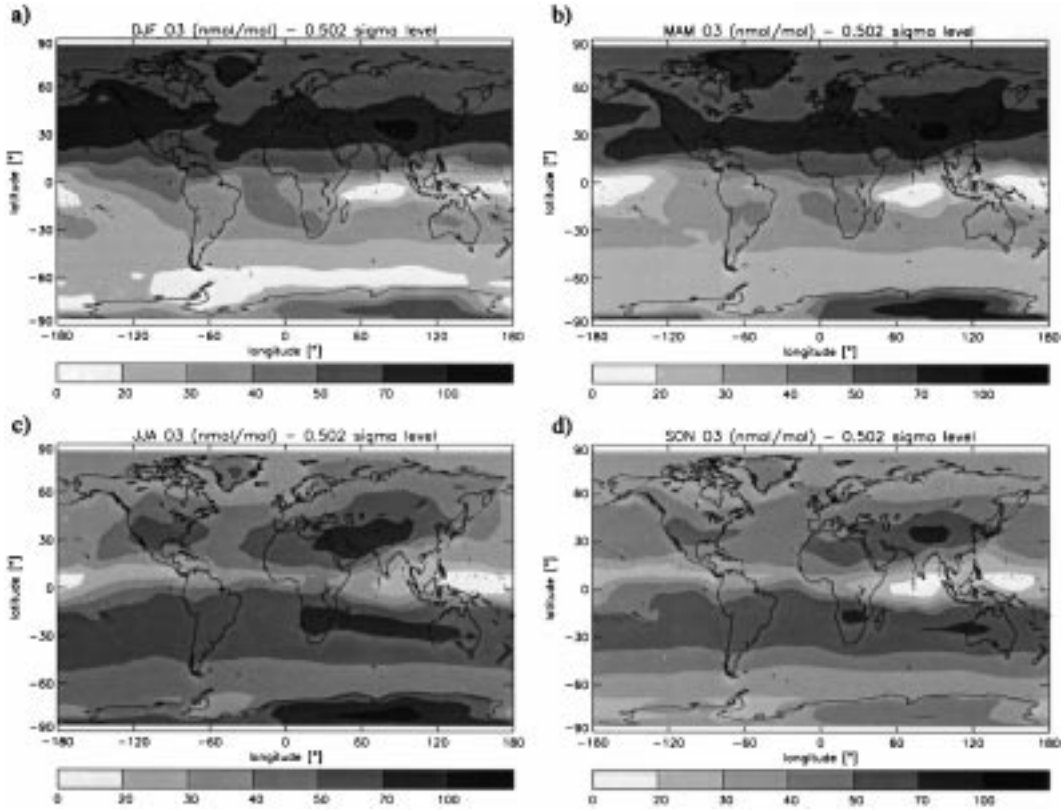

Fig. 5. The MATCH 0.502 sigma level seasonal mean O_3 distribution: (a) DJF, (b) MAM, (c) JJA, (d) SON. The data corresponds to an approximate pressure level of 500 hPa.

by high water vapor concentrations in the tropics, favoring reaction R3.

The manner in which this maximum follows the progression of the sun from south of the equator in December–January to north of the equator in June–August can clearly be seen in Fig. 8. One of the best means we have of determining whether the OH levels are approximately correct is by using them to compute lifetimes of various trace gases against attack by the OH radical. For the distribution shown in Figs. 7, 8, we compute a CH_4 lifetime of 9.0 years. This is in good agreement with the recent estimate by Krol et al. (1998), who first used observed CH_3CCl_3 concentrations to scale their modeled OH distribution and then used this "corrected" OH distribution to obtain a CH_4 lifetime from reaction with OH of 9.2 years in 1978, and 8.6 years in 1993. Our calculated CH_4 lifetime resulting from reaction with OH thus agrees quite well with those of Krol et al. (1998), verifying the main features and approximate absolute values of the calculated OH distributions.

3.3. *Tropospheric budgets of CO, CH_4, HO_x radicals and H_2O_2*

The high OH concentrations in tropical regions shown in Figs. 7, 8 would lead one to expect that CO and CH_4 will be oxidized predominantly in these regions. This is indeed computed by

Fig. 6. Comparison of observed seasonal mean O_3 profiles with those computed by MATCH for four representative stations which may best represent background chemistry. The boxes are observed O_3; the solid line depicts the MATCH O_3 levels. The name and location of each site is given above each set of seasonal mean plots.

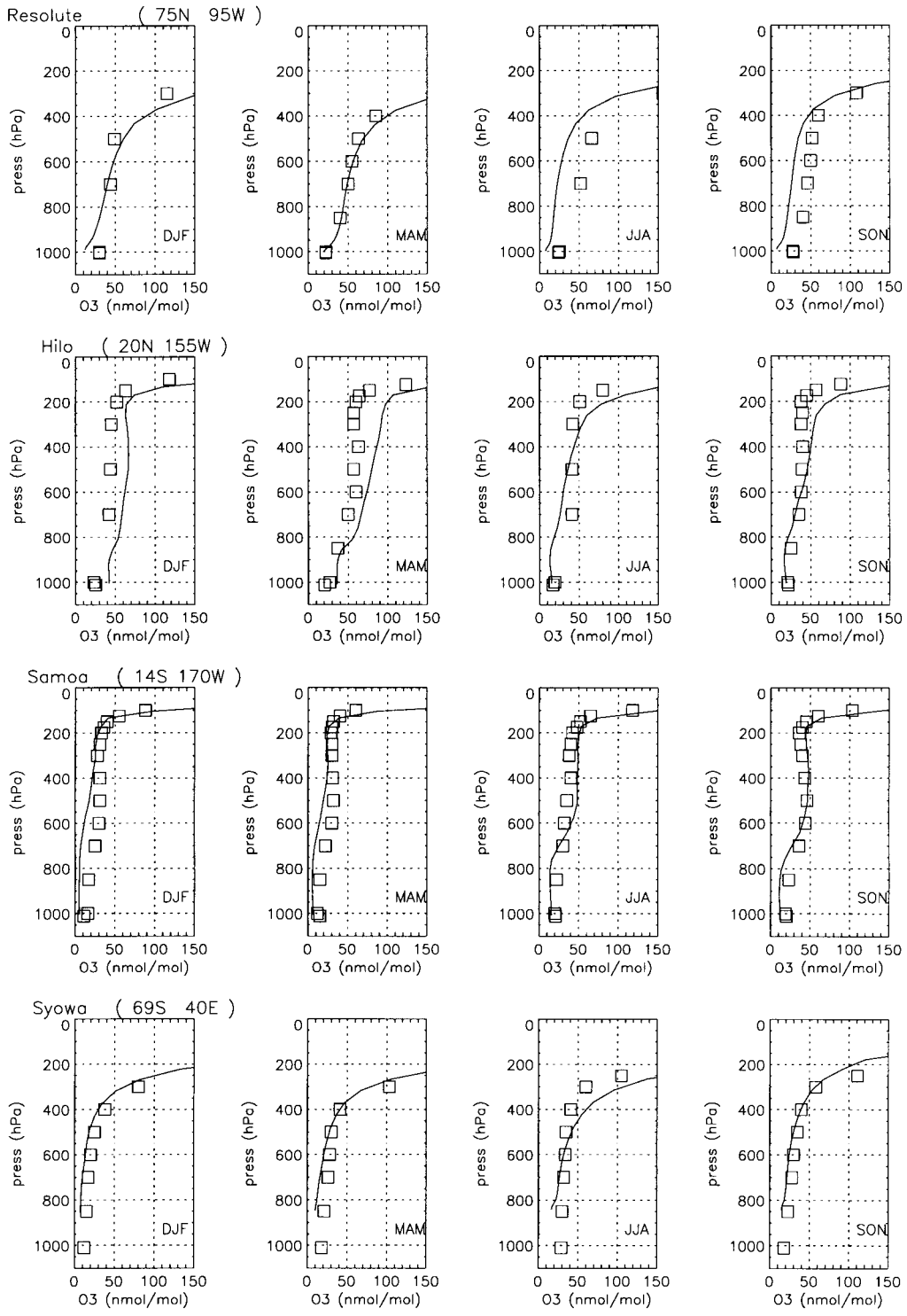
Resolute (75N 95W)
Hilo (20N 155W)
Samoa (14S 170W)
Syowa (69S 40E)
DJF
MAM
JJA
SON
press (hPa)
O3 (nmol/mol)
0
200
400
600
800
1000
0 50 100 150

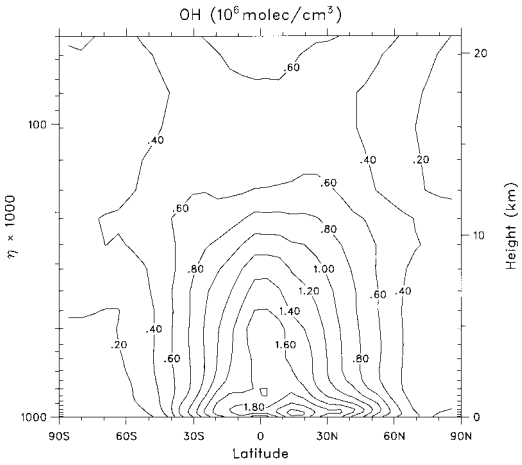

Fig. 7. Annual zonal mean (24-h average) OH distribution as computed by MATCH.

MATCH, as shown in Fig. 9. The degree to which the oxidation of these two gases is focused towards the tropics is remarkable. For CO, which has a lifetime of about a month in the tropics, this implies major production of CO over the continental tropics (very little is emitted by the oceans), as CH_4 oxidation alone would only sustain about 40 nmol/mol, while observations are closer to 100 nmol/mol. Important additional CO sources are oxidation of reactive hydrocarbons, such as isoprene, and biomass burning during dry seasons. The concentration of CH_4 oxidation towards the tropics also has another reason in addition to the higher tropical OH concentrations: the $CH_4 + OH$ rate coefficient increases with temperature.

Globally averaged chemical fluxes in the CH_4 oxidation sequences which lead via CH_2O to CO and further on to CO_2 are shown in Fig. 1. The fluxes are normalized by the first step, $CH_4 + OH$ (R13), consuming 455 Tg CH_4/year in the troposphere, or globally averaged 1.06×10^{11} molecules $cm^{-2}\,s^{-1}$, for which we substitute 100 units flowing into CH_3O_2. 159 units are leaving this intermediate reservoir, the 59 units of enhancement being due to a branch of recycling from CH_3O_2H via reaction R17b to CH_3O_2 (reaction sequence C6). The net result of these recycling reactions is a loss of OH and HO_2; globally averaged the reaction cycle C6 leads to the destruction of ca. 0.6 OH and 0.6 HO_2 radicals (1.2 HO_x) per CH_4 molecule oxidized. In the continental troposphere with higher NO_x levels the competing reaction R14 reduces the importance of C6 and its effect on HO_x (-0.8 HO_x per oxidized CH_4).

Counting the losses and gains of HO_x radicals in Fig. 1, we note up to the formation of CO a loss of 172 units of OH, but a gain of 74 units of HO_2. Altogether the conversion of CH_4 to CO causes a net loss of 98 units of HO_x. Further oxidation of CH_4-derived CO to CO_2 converts 96 units of OH to HO_2 without HO_x destruction. Note that another 154 units of CO oxidation and OH to HO_2 conversion are due to CO sources other than CH_4 oxidation.

Globally averaged every conversion of CH_4 to CO_2 thus causes an overall loss of about 2.7 OH and an overall production of about 1.7 HO_2, which amounts to a net loss of 1.0 HO_x. Again these numbers strongly depend on NO_x concentrations: for the continental troposphere the OH loss is practically the same, but net HO_2 production increases to 2.3 per oxidized CH_4 which reduces the net loss of HO_x to 0.4.

Fig. 10 shows the globally averaged reaction fluxes for OH and HO_2 radicals in the troposphere scaled to the primary production of OH from $O(^1D) + H_2O$ (100 units). The corresponding absolute numbers in molecules $cm^{-2}\,s^{-1}$ are shown in Figs. 11, 12 which list the major contributions to gross production, P, and loss, L, of OH and HO_2 radicals. Besides the global average these figures also show values for the subsections northern/southern hemisphere and continental/marine troposphere.

The conversion of CH_4 to CO_2 is the dominant sink of OH radicals in the global troposphere. According to the model results, about 18% of the OH radicals react with CH_4 and another 33% with its oxidation products, CH_3O_2H, CH_2O and CO, adding up to 51%; 27% react with CO that comes from other sources than CH_4 oxidation, and the remaining 22% react with inorganic species like HO_2, H_2, H_2O_2 and O_3. Note that these numbers may look very different in continental boundary layer air masses, where non-methane hydrocarbons (NMHC) like isoprene and other biogenic or anthropogenic volatile organic compounds (VOC) may be the dominant sink for OH radicals (Houweling et al., 1998; Wang et al., 1998). For the background chemistry of the free troposphere, however, CH_4 and CO are still dominant.

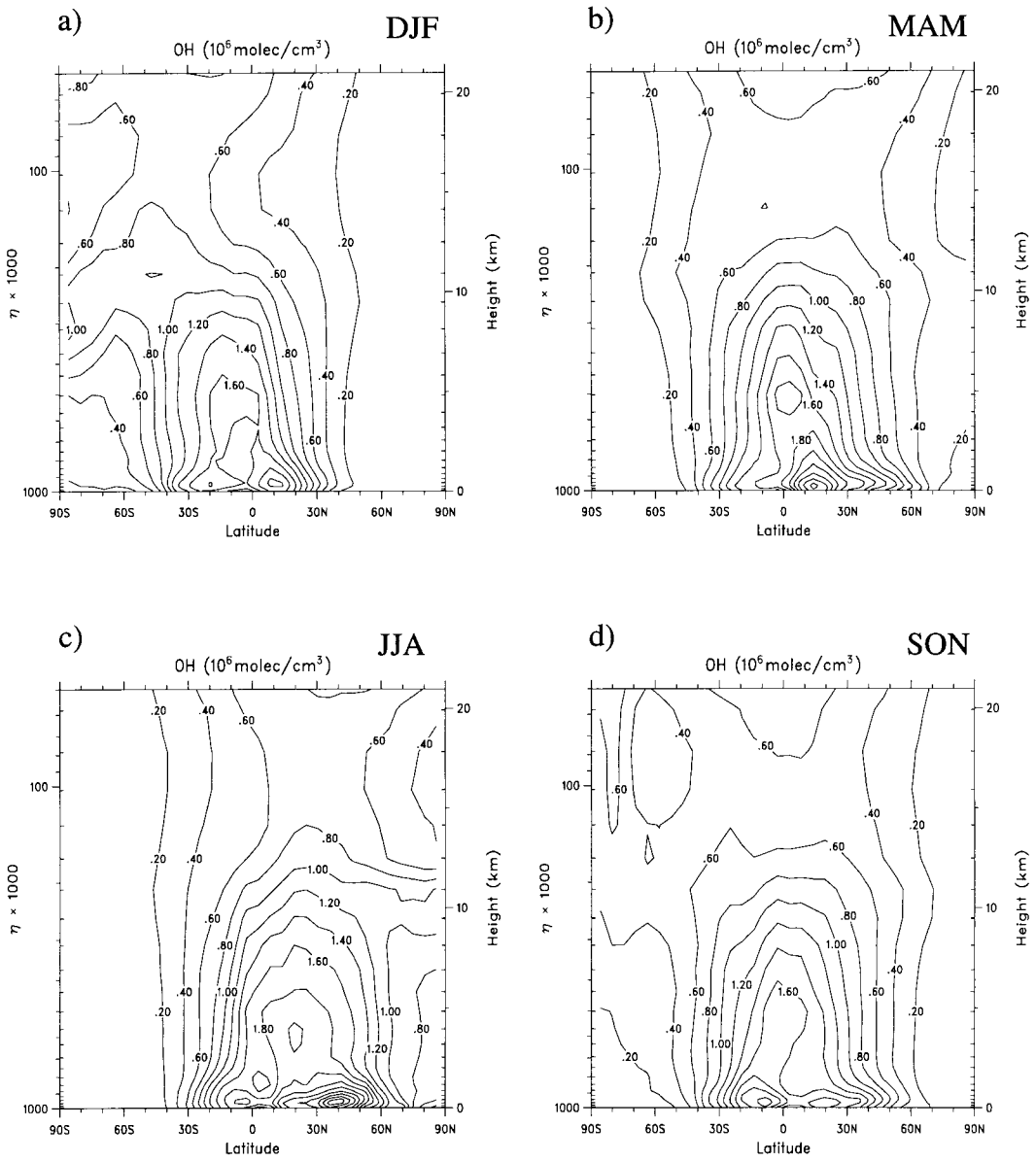

Fig. 8. Seasonal zonal mean (24-h average) OH distribution as computed by MATCH: (a) DJF, (b) MAM, (c) JJA, (d) SON.

While some processes like the reaction of OH with HO_2 or reaction cycles like C6 lead to the net loss of two HO_x radicals (radical chain terminating reactions), most reactions and reaction sequences shown in Fig. 10 lead to an interconversion of OH and HO_2 without net radical loss (radical chain propagating reactions). This interconversion may occur within one reaction step (e.g., R4 and R5) or via reaction sequences of intermediates like methyl peroxy radicals (sequence C3), the hydroperoxides H_2O_2 and CH_3O_2H (C4) or formaldehyde CH_2O (C7b).

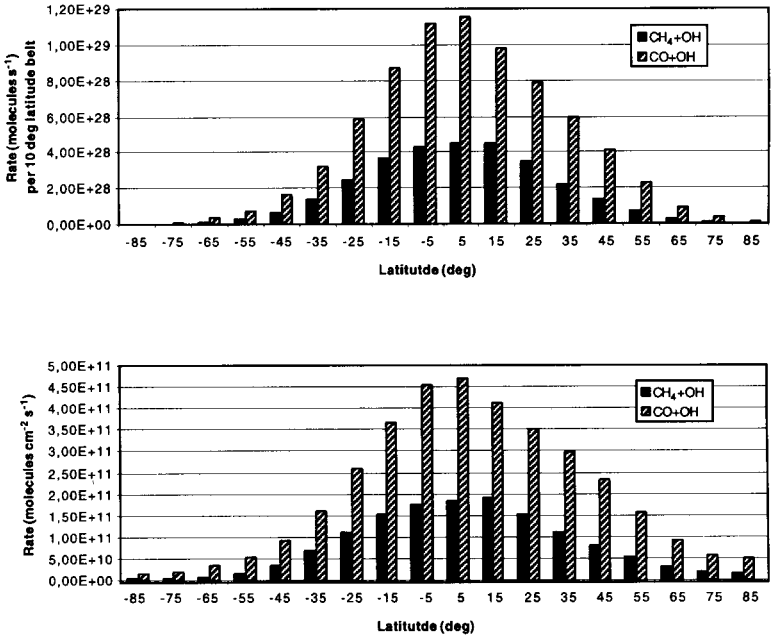

Fig. 9. Rates of CH_4 and CO oxidation by OH for 10° latitude belts; the rates are given as both volume-integrated (top panel) and column-integrated (bottom panel) totals, showing the distinct effects of the OH distribution and the greater surface area in the tropics (the volume integrated rates in units of molecules s^{-1} were obtained by multiplication of the mean column integrated reaction rate with the surface area of each latitude belt).

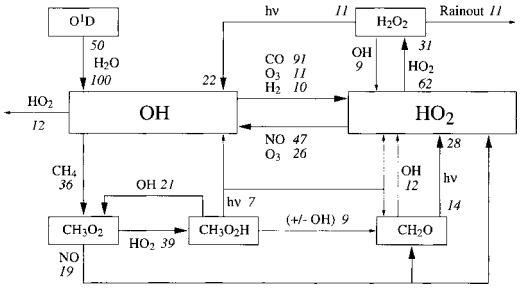

Fig. 10. HO_x reaction cycle budgets. Reaction rates for the global troposphere are scaled to the primary production of OH (100, corresponding to a globally averaged flux of 2.9×10^{11} molecules $cm^{-2}\,s^{-1}$); minor pathways (<5) and the formation and destruction of HNO_4 are neglected, as the net effect on HO_x is small. Note that because of recycling another 102 units enter the OH pool, in other words, gross production and loss of OH are each about twice as large as the primary production from $O(^1D) + H_2O \rightarrow 2OH$.

Consequently, gross production and loss of HO_x radicals are much larger than the primary production from $O^1D + H_2O$. Globally averaged the total production of OH [P(OH)] is about twice the primary production by $O^1D + H_2O$, and the same is almost true for the total production of HO_2 [$P(HO_2)$]. In the continental troposphere the enhancement factors are 2.4 and 2.6, respectively. If direct interconversion of OH and HO_2 is not taken into account, $P(HO_x)$ is somewhat smaller than P(OH) or $P(HO_2)$ but still almost twice the primary production rate (Fig. 13).

Fig. 14 shows the budget for hydrogen peroxide, one of the key species in the cycling of HO_x radicals. Globally averaged our model results show the formation of H_2O_2 as the major loss term of HO_2, competing with R5 which dominates in the NO_x-richer continental troposphere. In the gas phase H_2O_2 undergoes only two major reactions: either it photolyses yielding two OH radicals or it reacts with OH. The latter leads to the net destruction of 2 HO_x radicals in a cycle equivalent to sequence C6. On the other hand H_2O_2 is a highly soluble compound which is removed from the atmosphere by rainout; also in this case it acts as a net sink for HO_x radicals. In Fig. 14, the segment "Transport/ Deposition" is the difference between chemical production and loss of H_2O_2, which is largely due to

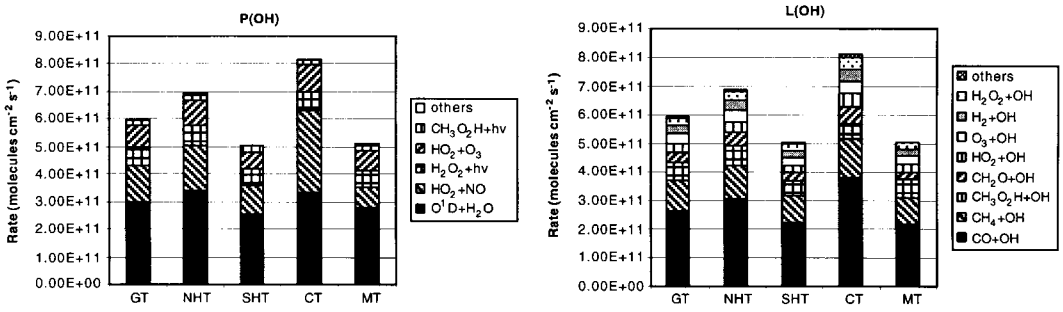

Fig. 11. Globally averaged gross production (left panel) and loss (right panel) fluxes of OH radicals in molecules/cm^2/s, for the global troposphere (GT) and its subsections northern hemisphere (NHT), southern hemisphere (SHT), continental troposphere (CT) and marine troposphere (MT). The listing includes the reaction rates of the major pathways shown in Fig. 10; the relatively small segment "others" mainly consists of formation and destruction of HNO_3 and HNO_4. Note that for this and all following bar figures, the order of reactions in each bar is the same as the order of reactions in the legend.

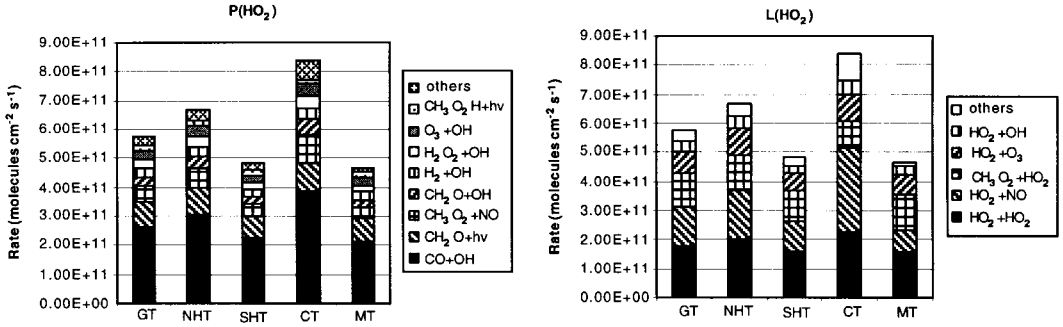

Fig. 12. Gross production (left panel) and loss (right panel) of HO_2 radicals. The listing includes the reaction rates of the major pathways shown in Fig. 10; the segment "others" is dominated by formation and decomposition of HNO_4.

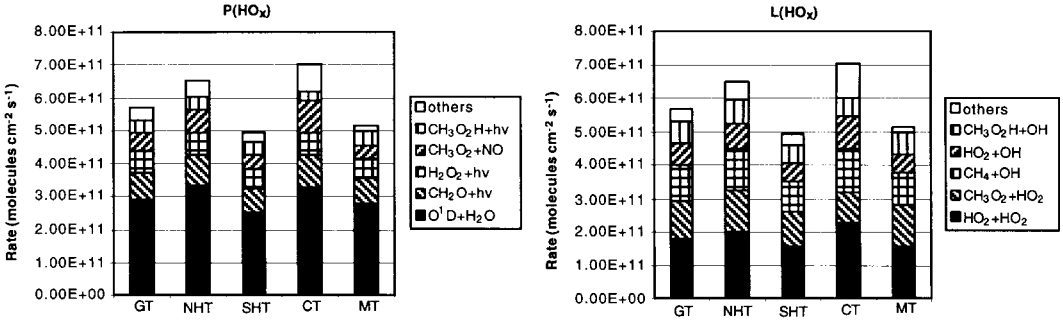

Fig. 13. Gross production (left panel) and loss (right panel) of HO_x radicals ($OH + HO_2$). The listing does not include direct interconversions between OH and HO_2.

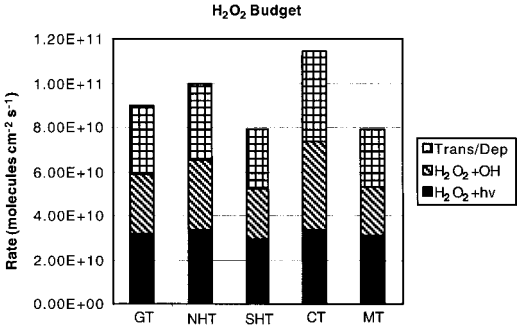

Fig. 14. H_2O_2 Budget. The column heights correspond to chemical production of H_2O_2 via $HO_2 + HO_2 \rightarrow H_2O_2 + O_2$; the segment "Transport/Deposition," largely due to rainout, is the difference between production from the HO_2 self-reaction and photochemical loss via $H_2O_2 + OH \rightarrow H_2O + HO_2$ and $H_2O_2 + h\nu \rightarrow 2OH$.

rainout. In aqueous phase cloud chemistry, which was not considered in our model, H_2O_2 acts as a strong oxidant; for example, it can significantly contribute to the conversion of S(IV) to S(VI), as analyzed by Roelofs et al. (1998). Loss of H_2O_2 by this reaction, however, is less than 10^{10} molec/cm^2/s, and therefore not very significant for H_2O_2.

3.4. *The ozone budget in the troposphere*

The tropospheric reactions which influence O_3 were discussed earlier in this work. Ozone can either be formed or destroyed by in situ reactions in the troposphere, largely depending on NO levels. A large fraction of the actual gross production and loss of O_3 molecules occurs in cycles without net ozone change, primarily through reactions R1 + R2 and reactions R10 + R6 + R7, as discussed before. The net chemical production of ozone is only a very small fraction of these large numbers. To avoid numerical problems, such numerically dominant null cycles can be eliminated by application of the odd oxygen family concept. The gross chemical production and loss terms of ozone which we will discuss below are based on the following definition of the odd oxygen family: $O_x = O_3 + O + O(^1D) + NO_2 + 2NO_3 + 3N_2O_5 + HNO_3 + HNO_4$. The sum O_x is dominated by the O_3 term, so that the rate of change of O_3 is to a very good approximation equal to that of O_x. This approximation applies to the background chemistry as discussed in this paper. In highly polluted regions containing much NO_y it may not be very accurate. The introduction of the O_x family concept allows the calculation of gross ozone production and loss terms, $P(O_3)$ and $L(O_3)$, which reject the contributions from quantitatively large null cycles, especially the aforementioned reaction sequences R1 + R2 and R10 + R6 + R7. The difference between the gross production and loss terms equals the net chemical production of ozone, $P(O_3)_{net}$:

$$P(O_3)_{net} = P(O_3) - L(O_3). \quad (1)$$

Using the odd oxygen concept defined above, $P(O_3)$ is dominated by the reactions R5 and R14, while $L(O_3)$ is dominated by R3, R8; and R9. They can thus be approximated as:

$$P(O_3) \approx k_5[HO_2][NO] + k_{14}[CH_3O_2][NO], \quad (2)$$

$$L(O_3) \approx k_3[O(^1D)][H_2O] + k_8[HO_2][O_3] + k_9[OH][O_3], \quad (3)$$

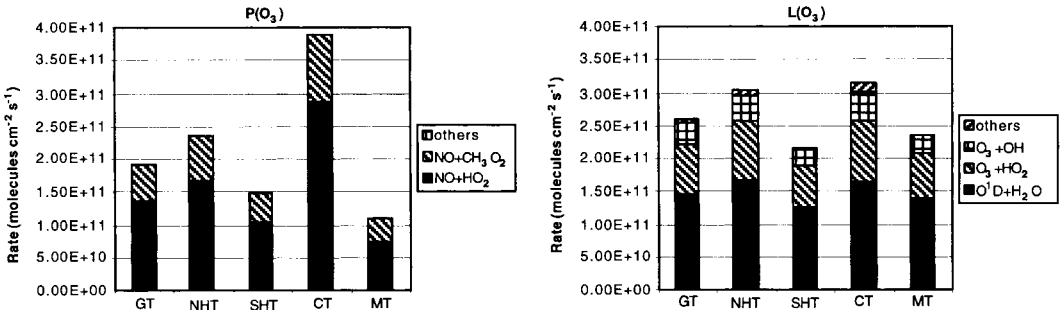

Fig. 15. Gross production (left panel) and loss (right panel) fluxes of ozone; the segment 'others' accounts for production and loss terms of the NO_y species included in the definition of odd oxygen, particularly HNO_3 and HNO_4 (see text). The individual contributions by the reactions are indicated by the vertical bars.

where the k terms are the rate coefficients and the square brackets stand for concentrations. In Fig. 15, we depict the individual contributions of these reactions to $P(O_3)$ and $L(O_3)$ in various regions of the troposphere, as computed by MATCH. It is seen that throughout the troposphere, reaction R5 is the dominant production term, and R3 is the dominant loss term; however, the rôles played by the other reaction pathways indicated in eqs. (2) and (3) are by no means negligible. The most remarkable feature in this figure is the great difference between $P(O_3)$ in the continental and the marine troposphere. This is due to the much higher NO_x mixing ratios over land (where most NO_x emissions occur). This is also reflected in the difference between the northern (NH) and southern hemispheres (SH), since NO_x emissions are larger in the NH. As partial compensation, there is also a tendency for more photochemical O_3 destruction in the NH and over continental regions. This is caused by the higher O_3 mixing ratios (which thus allow more O^1D formation, and therefore more ozone destruction via R3), as well as higher HO_x concentrations in these regions.

The net photochemical O_3 tendency, $P(O_3)_{net}$, has been calculated based on the output from the MATCH run, as shown in Fig. 16, and listed in Table 1 (in units of both molec/cm^2/s and $Tg(O_3)$/yr). The $P(O_3)$ and $L(O_3)$ terms are also replotted for reference; they are considerably larger than $P(O_3)_{net}$. In this simulation with MATCH, we compute net O_3 loss ($P(O_3)_{net} < 0$) for all of the regions considered except the continental troposphere, where the very high $P(O_3)$ values lead to net ozone production ($P(O_3)_{net} > 0$). A surprising result seen here is that, despite the significant difference in the continental and marine regions for $P(O_3)_{net}$, there is hardly any difference in the net O_3 production rates for the NH and SH.

The other two major factors contributing to the ozone budget in the troposphere, transport and surface deposition, are also depicted in Fig. 16. These terms balance the $P(O_3)_{net}$ term, as the tropospheric ozone content does not change significantly from one year to the next. For this run, we found a rather large stratosphere-troposphere exchange contribution of 1.13×10^{11} molec/cm^2/s, corresponding to 1450 $Tg(O_3)$/yr for the global troposphere. This is more than two times larger than most currently available estimates of the downward flux through the tropopause, e.g., 3.5×10^{10} molec/cm^2/s (Murphy and Fahey, 1994), 4×10^{10} molec/cm^2/s (Gettelman et al., 1997), 6.2×10^{10} molec/cm^2/s (Tie and Hess, 1997) and 5.7×10^{10} molec/cm^2/s (Beekmann et al., 1997, who considered only tropopause folds in the NH), and is at the upper limit of the range of $0.75–1.13 \times 10^{11}$ molec/cm^2/s computed by Ebel et al. (1996), who examined statistics from global analyses for an 8-year period (the range stated here is based on their range of $1.0–1.5 \times 10^{11}$ molec/cm^2/s for the NH, and their finding that the exchange in the NH is about twice that in the SH). It is important to realize that most of these studies focus on STE due to tropopause folding events, mainly near the mid-latitude jet streams, whereas MATCH seems to predict the primary

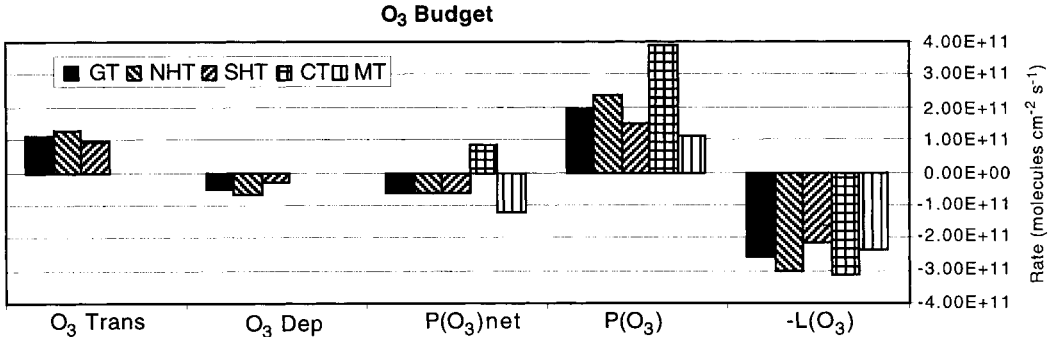

Fig. 16. Annually averaged ozone budget. The terms considered are: transport from the stratosphere and from the other hemisphere (O_3 Trans), surface deposition (O_3 Dep), net chemical production [$P(O_3)_{net}$], and gross photochemical production [$P(O_3)$] and loss [$L(O_3)$]. The corresponding data values are listed in Table 1.

Table 1. *The tropospheric O_3 budget as computed by MATCH*

Process	GT	NHT	SHT	CT	MT
(10^{10} molec/cm^2/s)					
net transport[a)]	11.2	12.8	9.6	—	—
dry deposition	−4.9	−6.5	−3.2	—	—
$P(O_3)_{net}$	−6.3	−6.3	−6.4	8.2	−12.3
$P(O_3)$	19.4	23.8	15.0	39.5	11.2
$-L(O_3)$	−25.7	−30.1	−21.4	−31.3	−23.5
(Tg(O_3)/yr[b)])					
net transport[a)]	1440	820	620	—	—
dry deposition	−620	−420	−210	—	—
$P(O_3)_{net}$	−810	−400	−410	310	−1120
$P(O_3)$	2490	1530	960	1480	1020
$-L(O_3)$	−3300	−1930	−1370	−1170	−2130

The regions are: global troposphere (GT), northern hemisphere troposphere (NHT), southern hemisphere troposphere (SHT), continental troposphere (CT) and marine troposphere (MT).
[a)] The net transport term gives the STE flux for the GT, and the STE flux plus the interhemispheric exchange flux for the NHT and SHT regions; the net transport term (as well as dry deposition) could not be computed individually for the CT and MT for this version of MATCH.
[b)] Numbers rounded off to the nearest tens position.

influx (presumably along isentropes) near the subtropical tropopause break (seen earlier in Subsection 3.1). A similar pattern of STE flux primarily near the subtropical tropopause break was also computed by the ECHAM global model (Roelofs and Lelieveld, 1995). The reason behind this discrepancy is not yet clear, though it seems likely that it is at least in part due to the fact that global models cannot resolve tropopause folding events, which occur on scales much smaller than the typical 100+ km model grid cell dimensions.

Despite the sizeable and perhaps even incorrectly located O_3 influx in our simulation, we still obtain O_3 profiles which are within reason compared to observations, as presented earlier (which is likely in part due to the compensating effect of too low NO_x levels in these runs, as indicated earlier). This very large influx of O_3 is not completely balanced by global surface uptake of O_3 in our computations ($\mathrm{Dep}(O_3) = -0.49 \times 10^{11}$ molec/cm^2/s). Thus, in order to balance equation (4), $P(O_3)_{net}$ must be negative; in this run, we computed $P(O_3)_{net} = -0.63 \times 10^{11}$ molec/cm^2/s. A final note is important to make here about the global O_3 budget: even though we compute a relatively large influx of O_3 into the troposphere, this term is still much exceeded by the gross photochemical loss and production terms ($P(O_3)$ and $L(O_3)$), which are important in controlling the O_3 distribution in much of the troposphere (as will be demonstrated in Subsection 3.5).

We can also calculate the $P(O_3)$ and $L(O_3)$ terms for every grid element in our global model, and thus depict the distribution of these terms for any desired region. In Fig. 17, we show the $P(O_3)$, $L(O_3)$, and $P(O_3)_{net}$ terms as zonal annual means from the MATCH run. The O_3 production term P shows highest values (exceeding 5 nmol/mol/day) in the lowest few kilometers of the troposphere, especially at mid-latitudes of the northern hemisphere. This results from the strong emissions of NO catalysts by fossil fuel burning. The largest ozone destruction rates are calculated for the lower 5 km of the tropical troposphere with values greater then 2 nmol/mol/day. Most ozone loss is coming from reactions R1 and R3, the same reactions that also produce hydroxyl radicals. This term peaks in the tropics because of a maximum in water vapor concentrations and a minimum in vertical ozone columns, which allows maximum penetration of $O(^1D)$-producing photons.

Fig. 17c shows net ozone production near the surface at most latitudes, and in the middle to upper tropical troposphere; in the rest of the troposphere, net loss dominates. The turnaround point from net loss to net production is at about 7–8 km near the equator, in good agreement with studies based on observed trace gas profiles

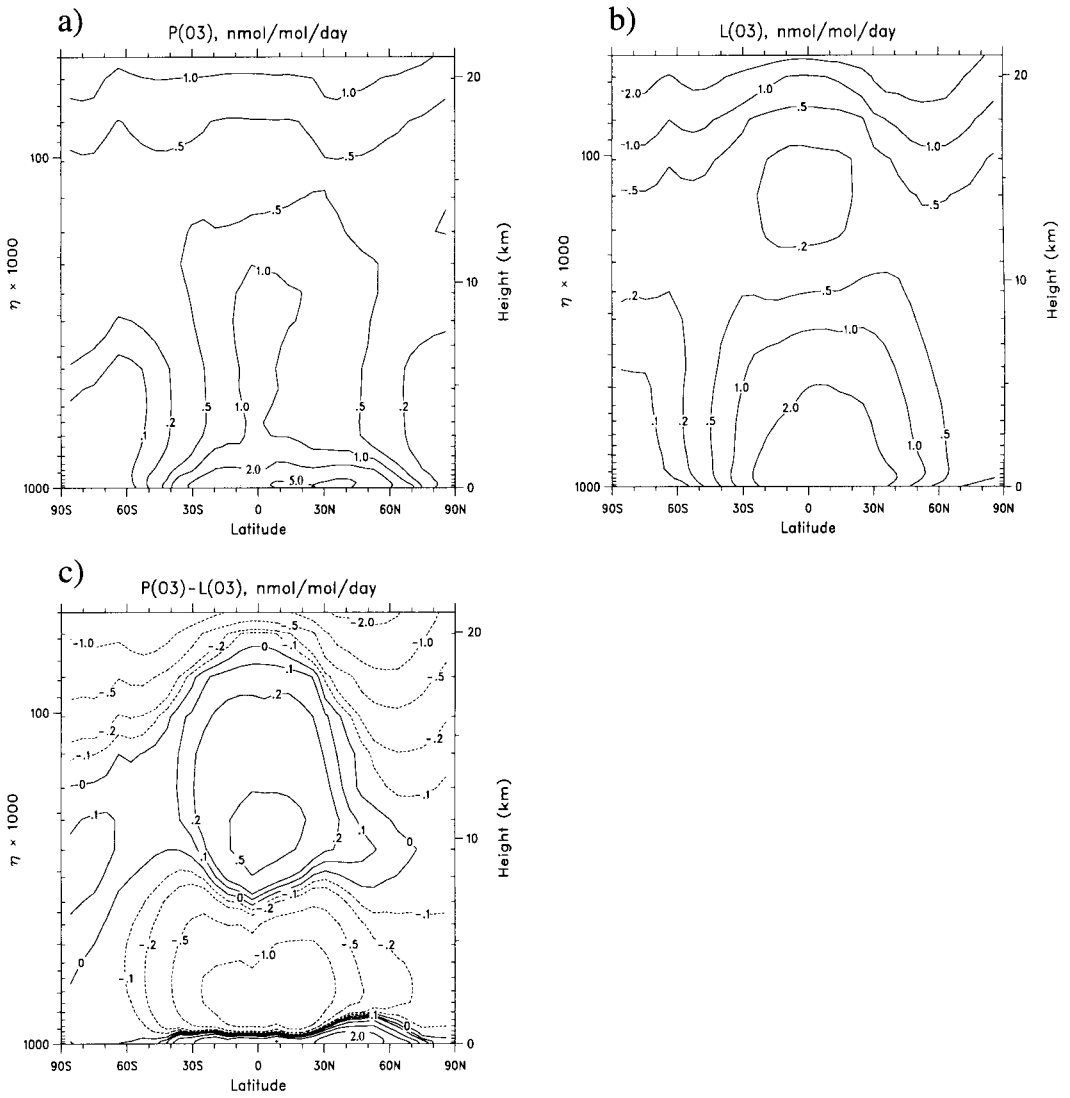

Fig. 17. Depiction of the annual zonal mean O_3 production and destruction terms in nmol/mol/day as computed by MATCH: (a) gross ozone production ($P(O_3)$); (b) gross ozone loss [$L(O_3)$]; and (c) net ozone production [$P(O_3) - L(O_3)$], where the dotted lines in panel (c) indicate negative contours (net destruction).

(Schultz et al., 1998). On the other hand, the region of net loss covers a much greater extent of the free troposphere than found in the study of Wang et al. (1998).

In order to interpret the net O_3 production computed by MATCH (Fig. 17c), it is important to consider the global NO_x distribution, depicted in Fig. 18. This shows high mixing ratios near the surface at northern mid latitudes, due to the large anthropogenic NO_x sources there, low levels in the mid troposphere, and increasing mixing ratios at higher altitudes, due to lightning and convective pumping of soil and biomass burning emissions. The correspondence between Figs. 18 and 17c is clear: where NO_x levels are high, the net O_3 tendency is positive, elsewhere the net O_3 tendency is negative. For the free troposphere, the zero isoline for O_3 net tendency and the 20 pmol/mol

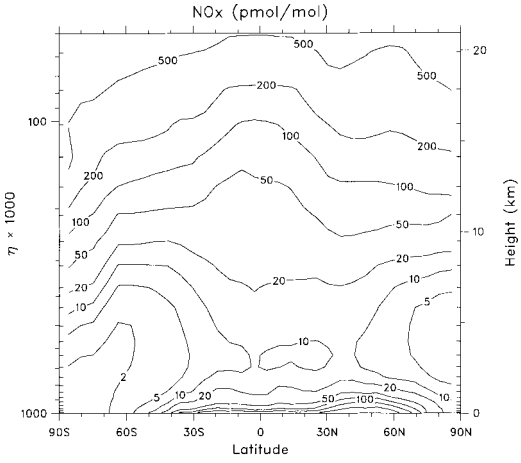

Fig. 18. The annual zonal mean NO_x distribution computed by MATCH.

line for the NO_x mixing ratio lie very close to each other; nearer the surface, the zero net tendency line is in closer agreement with the 50 pmol/mol NO_x line. This implies that for our computations, the average value for the "critical" NO_x mixing ratio, where the net O_3 tendency switches from loss to production, is about 20 pmol/mol in the free troposphere, and 50 pmol/mol near the surface. We indicated earlier that the global NO_x mixing ratios computed in this MATCH run appear to be somewhat low compared to observations. This would imply that in all likelihood, the net photochemical O_3 tendency is positive in more of the free troposphere than indicated in Fig. 17c (in accord with the findings of Wang et al., 1998). Despite this, however, we nevertheless find that photochemistry has a significant degree of control over the O_3 distribution in our model, as demonstrated in the Subsection 3.5.

3.5. *The significance of in-situ tropospheric ozone production*

Until about 25 years ago, it was believed that nearly all tropospheric O_3 originated in the stratosphere and was essentially inert in the troposphere, only being lost by surface uptake (Fabian and Junge, 1970). We now know, for instance from earlier analyses by Crutzen and Gidel (1983), who examined global 2D model simulations with and without in situ photochemical O_3 production, and the 3D budget analyses presented in the previous sections, that this is not the case. To illustrate this very convincingly we show results from a simulation with MATCH which we performed to emphasize the relative influence of stratospheric influx and in-situ O_3 production. For this run, we reduced ozone mixing ratios in the model stratosphere to only 10% of their normal values (retaining, however, the original stratospheric ozone for photolysis rate calculations). This had the effect of reducing the net flux of O_3 into the troposphere to less than 8×10^9 molec/cm^2/s, which is almost negligible compared to the flux in our base run, which was noted earlier to be about 1.1×10^{11} molec/cm^2/s. For our analysis, we have defined a "chemical tropopause" as the layer in which the monthly mean O_3 mixing ratio is 150 nmol/mol (we have found that this chemical tropopause can be closely approximated by the formula $P_t(\text{hPa}) = 300 - 215\cos(\phi)$, where ϕ is the latitude). The region below this layer is considered to be the troposphere. We then compute the STE flux as the net transport tendency for the troposphere. Specifically, we do this by computing the mass of ozone in the troposphere before (M_b) and after (M_a) the transport part of the model time step. The difference $M_a - M_b$ represents the net effect of transport on tropospheric O_3, which can be summed for each time step over a run to give the net STE influx term for the troposphere. It is important to realize that this net flux is actually the difference between two somewhat larger fluxes, a flux of ozone from the troposphere to the stratosphere in the tropical upwelling regions (i.e., a negative flux for the troposphere), and a downward flux of ozone from the stratosphere to the troposphere (i.e., positive for the troposphere), which occurs predominantly at middle to higher latitudes, particularly near the jet stream and through the subtropical tropopause breaks.

The resulting ratio of O_3 for this run compared to that in the base run is shown for January and July conditions in Fig. 19. In July, polewards of 40 N, the O_3 mixing ratio near the surface in this run is over 90% as high as it was in the base run, and over 70% as high throughout most of the northern hemisphere troposphere below 5 km. In January in the SH, these numbers are not quite as extreme, but still significant, with about 60–80% of the O_3 levels from the full-strato-

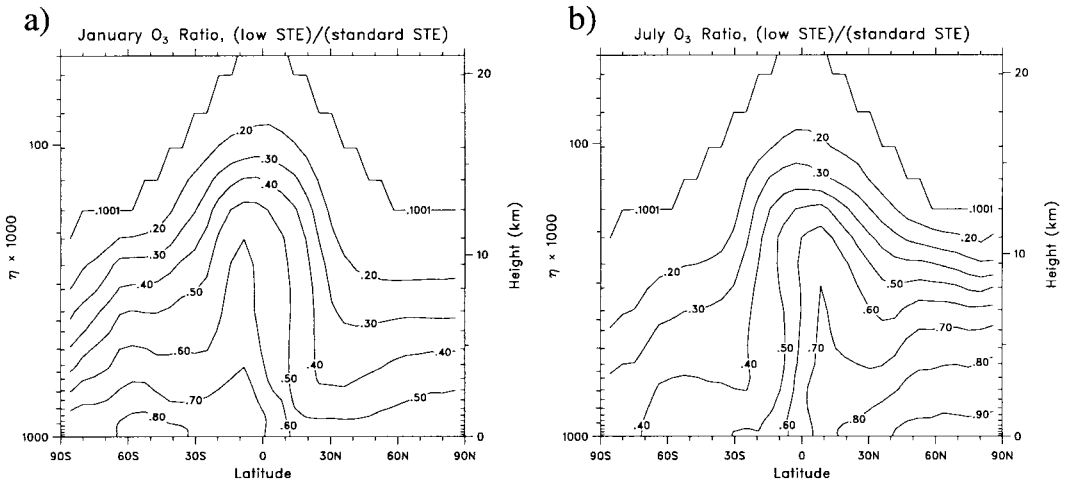

Fig. 19. The zonal mean ratio of O_3 concentrations from a MATCH run in which stratospheric O_3 is reduced to 1/10 of its normal mixing ratios versus those from the base run: (a) January, (b) July.

spheric-flux run still being present. This indicates that in our base run, it is in-situ photochemistry, not stratospheric influx, which primarily controls O_3 throughout the lower half of the troposphere in both hemispheres during summer months. In the winter months, on the other hand, the addition of the STE flux is quite important for surface level ozone, increasing ozone mixing ratios by a factor of 2–3 compared to the run with negligible influx. Nevertheless, this means that even in winter, 1/3–1/2 of the ozone in the lower troposphere would be present even if there were only a negligible influx from the stratosphere.

This is a remarkable result, especially when one reflects on the very high net O_3 influx from the stratosphere and low NO_x concentrations which we compute in our base run with MATCH. Our STE source of 1.1×10^{11} molec/cm^2/s, although still possibly acceptable, is at the upper limit of current estimates of the net influx (Ebel et al., 1996). This means that in all likelihood, the influence of stratospheric influx is overestimated in our base run, affecting ozone especially in the upper half of the troposphere. Our conclusion about the tremendous significance of in situ ozone photochemistry in the troposphere relative to STE influx agrees with many earlier studies, and most recently with advanced 3D model studies by Roelofs and Lelieveld (1997) and Wang et al. (1998).

4. Conclusions

In this paper, we have given a largely tutorial overview of the photochemical processes in the background troposphere, the so-called O_3–NO_x–HO_x–CH_4–CO chemistry. These processes start with the absorption of solar ultraviolet radiation by ozone and the production of $O(^1D)$ atoms which can react with water vapor to produce OH radicals, the "detergents of the atmosphere". Almost all gases that are emitted to the atmosphere are removed by reaction with OH. OH radicals react mainly with CO, CH_4 and CH_4 oxidation intermediates, starting sequences of reactions in which ozone can be produced or destroyed depending on ambient NO levels. The CH_4 and CO oxidation cycles also play an important rôle in determining the concentrations of OH and the related species HO_2 and H_2O_2. Using the global chemistry-transport model MATCH we presented analyses of the global and hemispheric O_3, HO_x and H_2O_2 budgets in the troposphere. Results such as these are certainly model dependent. For the particular case presented in this paper, the numbers are influenced by the very high STE O_3 flux and the low NO_x levels, so that we have likely underestimated some of the key photochemical reaction rate terms (e.g., gross O_3 production). Nevertheless, we expect our results to represent

the main features of the atmospheric budgets of these gases. In fact, we have found that similar calculations performed with the MOGUNTIA model (Crutzen and Zimmermann, unpublished results) gave numbers which deviated at most by 30% from those presented here.

Our model calculations show that in-situ chemical gross production and destruction of ozone in the troposphere are larger than the downward flux from the stratosphere, even under our model conditions which probably overestimate the supply from the stratosphere. Furthermore, in a model run in which we reduced the stratospheric downward flux of ozone at middle and high latitudes to only about 10% of its base model values, we nevertheless calculated about 60–90% of the base case ozone concentrations in the lower half of the troposphere during summer in both hemispheres, most drastically in the northern hemisphere. This result clearly demonstrates that in-situ tropospheric photochemistry has a dominating influence on ozone levels in much of the troposphere, especially the lower troposphere. Nevertheless, it is important to bear in mind that the STE influx makes a major contribution to the total O_3 in the troposphere, since the O_3 mixing ratios tend to be much higher at greater altitudes, where the influence of STE influx on O_3 is most important. The additional rôle of NMHCs in producing O_3, which is neglected in our simulation, will result in even more control of in situ photochemistry on O_3 concentrations. According to Wang et al. (1998), addition of NMHC chemistry in their 3D model leads to about 15% more ozone in the remote troposphere, but a decrease in global mean OH concentrations by as much as 20%. The estimate about tropospheric ozone enhancement due to NMHC chemistry is close to the value calculated by Houweling et al. (1998) with another 3D model. These authors also calculated a depletion in OH concentrations over the continents, mostly due to isoprene-induced chemistry.

Finally, we note that the gross O_3 production (2460 $Tg(O_3)$/yr), destruction (3260 $Tg(O_3)$/yr) and stratospheric influx (1450 $Tg(O_3)$/yr) terms calculated in this study, and similarly large values in the above-mentioned models, are much larger than the estimated export of ozone of only 5 $Tg(O_3)$/yr from the polluted North American continent to the North Atlantic Ocean during summer (Parrish et al., 1993). Although the above budget numbers from global models are rather uncertain, there is one term, the loss of O_3 by reactions R1 and R3, equal to about 1500 $Tg(O_3)$/yr, which can be fairly well constrained based on global O_3 and H_2O distributions and well known photolysis parameters. This implies only a very small contribution of regional photochemical smog ozone to the global photochemical ozone budget, which appears to be dominated by background $O_3/CH_4/CO/HO_x/NO_x$ photochemistry.

5. Acknowledgements

We would like to thank Jos Lelieveld, Henning Rodhe, and an anonymous referee for valuable critical reviews which helped to improve this manuscript. Supercomputer time for MATCH development was provided by the EU SINDICATE project.

REFERENCES

Bates, T. S., Kelly, K. C., Johnson, J. E. and Gammon, R. H. 1995. Regional and seasonal variations in the flux of oceanic carbon monoxide to the atmosphere, *J. Geophys. Res.* **100**, 23,093–23,101.

Baughcum, S. L., Henderson, S. C., Hertel, P. S., Maggiora, D. R. and Oncina, C. A. 1987. *Stratospheric emissions effects database development*. NASA CR-4592, 1994.

Beekmann, M., Ancellet, G., Blonsky, S., DeMuer, D., Ebel, A., Elbern, H., Hendricks, J., Kowol, J., Mancier, C., Sladkovic, R., Smit, H. G. J., Speth, P., Trickl, T. and Van Haver, P. 1997. Regional and global tropopause fold occurrence and related ozone flux across the tropopause, *J. Atmos. Chem.* **28**, 29–44.

Benkovitz, C. M, Scholtz, M. T., Pacyna, J., Tarrason, L., Dignon, J., Voldner, E. C., Spiro, P. A., Logan, J. A. and Graedel, T. E. 1996. Global gridded inventories of anthropogenic emissions of sulfur and nitrogen. *J. Geophys. Res.* **101**, 29,239–29,253.

Crutzen, P, J. 1973. A discussion of the chemistry of some minor constituents in the stratosphere and troposphere. *Pure Appl. Geophys.* **106–108**, 1385–1399.

Crutzen, P. J. and Andreae, M. O. 1990. Biomass burning in the tropics: Impact on atmospheric chemistry and biogeochemical cycles. *Science* **250**, 1669–1678.

Crutzen, P. J. and Gidel, L. T. 1983. A two-dimensional photochemical model of the atmosphere (2) The tropospheric budgets of the anthropogenic chlorocarbons

CO, CH_4, CH_3Cl, and the effects of various NO_x sources on tropospheric ozone. *J. Geophys. Res.* **88**, 6641–6661.

Crutzen, P. J. and Zimmermann, P. H. 1991. The changing photochemistry of the troposphere. *Tellus* **43A/B**, 136–151.

DeMore, W. B., Sander, S. P., Howard, C. J., Ravishankara, A. R., Golden, D. M., Kolb, C. E., Hampson, R. F., Kurylo, M. J. and Molina, M. J. 1997. *Chemical kinetics and photochemical data for use in stratospheric modeling*. NASA JPL (Jet Propulsion Laboratory), Pasadena, California, USA.

Dentener, F. J. and Crutzen, P. J. 1993. Reaction of N2O5 on tropospheric aerosols: Impact on the global distributions of NO_x, O3, and OH. *J. Geophys. Res.* **98**, 7149–7163.

Dignon, J. and Penner, J. E. 1991. Biomass burning. A source of nitrogen oxides in the atmosphere. In: *Global biomass burning: atmospheric, climate, and biospheric implications* (ed. J. S. Levine). MIT Press, Cambridge, USA, 370–375.

Dlugokencky, E. J., Steele, L. P., Lang, P. M. and Masarie, K. A. 1994. The growth and distribution of atmospheric methane. *J. Geophys. Res.* **99**, 17021–17043.

Ebel, A., Elbern, H., Hendricks, J. and Meyer, R. 1996. Stratosphere-troposphere exchange and its impact on the structure of the lower stratosphere. *J. Geomag. Geoelectr.* **48**, 135–144.

Fabian, P. and Junge, C. E. 1970. Global rate of ozone destruction at the earth's surface. *Arch. Met. Geoph. Biokl., Serie A*, **19**, 161–172.

Fung, I. et al. 1991. Three-dimensional model synthesis of the global methane cycle. *J. Geophys. Res.* **96**, 13,033–13,065.

Gettelman, A., Holton, J. R. and Rosenlof, K. H. 1997. Mass fluxes of O_3, CH_4, N_2O, and CF_2Cl_2 in the lower stratosphere calculated from observational data. *J. Geophys. Res.* **102**, 19,149–19,159.

Ganzeveld, L. and Lelieveld, J. 1995. Dry deposition parameterization in a chemistry general circulation model and its influence on the distribution of reactive trace gases. *J. Geophys. Res.* **100**, 20,999–21,012.

Guenther, A. et al. 1995. A global model of natural volatile organic compound emissions. *J. Geophys. Res.* **100**, 8,873–8,892.

Hack, J. J. 1994. Parameterization of moist convection in the National Center for Atmospheric Research community climate model (CCM2). *J. Geophys. Res.* **99**, 5551–5568.

Hameed, S. and Dignon, J. 1991. Global emissions of nitrogen and sulphur oxides in fossil fuel combustion 1970–1986. *J. Air Waste Manage. Assoc.* **42**, 159–163.

Hao, W. M. and Liu, M.-H. 1994. Spatial and temporal distribution of tropical biomass burning. *Glob. Biogeochem. Cycles* **8**, 495–503.

Holtslag, A. A. M. and Boville, B. A. 1993. Local versus nonlocal boundary-layer diffusion in a global climate model. *J. Climate* **6**, 1825–1842.

Houweling, S., Dentener, F. and Lelieveld, J. 1998. The impact of nonmethane hydrocarbon compounds on tropospheric photochemistry. *J. Geophys. Res.* **103**, 10673–10696.

Kalnay, E., Kanamitsu, M., Kistler, R., Collings, W., Deavan, D., Gandin, L., Iredell, M., Saha, S., White, G., Woollen, J., Zhu, Y., Chelliah, M., Ebisuzaki, W., Higgens, W., Janawiak, J., Mo, K. C., Ropelewski, C., Wang, J., Leetmaa, A., Reynolds, R., Jenne, R. and Joseph, D. 1996. The NCEP/NCAR 40-year reanalysis project. *Bull. Am. Met Soc.* **77**, 437–471.

Kley, D., Crutzen, P. J., Smit, H. G. J., Voemel, H., Oltmans, S. J.,Grassl, H. and Ramanathan, V. 1996. Observations of near-zero ozone concentrations over the convective Pacific: Effects on air chemistry. *Science* **274**, 230–233.

Komhyr, W. D., Oltmans, S. J., Franchois, P. R., Evans, W. F. J. and Matthews, W. A. 1989. The latitudinal distribution of ozone to 35 km altitude form ECC ozonesonde observations, 1985–1987. In: *Ozone in the atmosphere* edited by R. D. Bojkov and P. Fabian, pp. 147–150.

Krol, M., Van Leeuwen, P. J. and Lelieveld, J. 1998. Global OH trend inferred from methylchloroform measurements. *J. Geophys. Res.* **103**, 10697–10711.

Landgraf, J. and Crutzen, P. J. 1998. An efficient method of online calculation of photolysis and heating rates. *J. Atmos. Sci.* **55**, 863–878.

Lawrence, M. G. 1996. *Photochemistry in the tropical Pacific troposphere. Studies with a global 3D chemistry-meteorology model.* Doctoral dissertation. Georgia Institute of Technology, 520 pp.

Lawrence, M. G. and Crutzen, P. J. 1998. The impact of cloud particle gravitational settling on soluble trace gas distributions. *Tellus* **50B**, 263–289.

Lawrence, M. G., Chameides, W.L., Kasibhatla, P.S., Levy, H., II and Moxim, W. 1995. Lightning and atmospheric chemistry: the rate of atmospheric NO production. In: *Handbook of atmospheric electrodynamics* (ed. H. Volland). CRC Press, Inc., Boca Raton, USA, 189–202.

Levy, H., II, 1971. Normal atmosphere: large radical and formaldehyde concentrations predicted. *Science* **173**, 141–143.

Levy, H., II, Mahlman, J. D., Moxim, W. J. and Liu, S. C. 1985. Tropospheric ozone: The rôle of transport. *J. Geophys. Res.* **90**, 3753–3772.

Mahowald, N. M., Rasch, P. J, Eaton, B. E., Whittlestone, B. and Prinn, R. G. 1997. Transport of 222 Radon to the remote troposphere using MATCH and assimilated winds from ECMWF and NCEP/NCAR. *J. Geophys. Res.* **102**, 28,139–28,152.

Michelson, H. A., Salawitch, R. J., Wennberg, P. O. and Anderson, J. G. 1994. Production of $O(^1D)$ from photolysis of O_3. *Geophys. Res. Lett.* **21**, 2227–2230.

Montzka, S. A. et al. 1996. Decline in the tropospheric abundance of halogens from halocarbons: Implications for stratospheric ozone depletion. *Science* **272**, 1318–1322.

Murphy, D. M. and Fahey, D. W. 1994. An estimate of the flux of stratospheric reactive nitrogen and ozone into the troposhere. *J. Geophys. Res.* **99**, 5325–5332.

Murphy, D. M., Fahey, D. W., Proffitt, M. H., Liu, S. C., Chan, K. R., Eubank, C. S., Kawa, S. R. and Kelly, K. K. 1993. Reactive nitrogen and its correlation with ozone in the lower stratosphere and upper troposphere. *J. Geophys. Res.* **98**, 8751–8773.

Olivier, J. G. J., Bouwman, A. F., Van der Maas, C. W. M., Berdowski, J. J. M., Veldt, C., Bloos, J. P. J., Visschedijk, A. J. H., Zandveld, P. Y. J. and Haverlag, J. L. 1996. *Description of EDGAR Version 2.0. A set of global emission inventories of greenhouse gases and ozone-depleting substances for all anthropogenic and most natural sources on a per country basis and on* 1×1 *grid.* RIVM/TNO report, December 1996. RIVM, Bilthoven, RIVM report nr. 771060 002 (TNO MEP report nr. R96/119).

Parrish, D. D., Holloway, J. S., Trainer, M., Murphy, P. C., Forbes, G. L. and Fehsenfeld, F. C. 1993. Export of North American ozone pollution to the North Atlantic Ocean. *Science* **267**, 1436–1439.

Price, C. and Rind, D. 1992. A simple lightning parameterization for calculating global lightning distributions. *J. Geophys. Res.* **97**, 9919–9933.

Price, C., Penner, J. and Prather, M. 1997. NO_x from lightning (1). Global distribution based on lightning physics *J. Geophys. Res.* **102**, 5929–5941.

Prinn, R. G. Weiss, R. F., Miller, B. R., Huang, J., Aylea, F. N., Cunnold, D. M., Fraser, P. J., Hartley, D. E. and Simmonds, P. G. 1995. Atmospheric trends and lifetime of CH_3CCl_3 and global OH concentrations. *Science* **269**, 187–190.

Rasch, P. J., Mahowald, N. M. and Eaton, B. E. 1997. Representations of transport, convection, and the hydrologic cycle in chemical transport models: Implications for the modeling of short lived and soluble species. *J. Geophys. Res.* **102**, 28127–28138.

Rasch, P. J. and Kristjansson, J. E. 1998. A comparison of the CCM3 model climate using diagnosed and predicted condensate parameterizations. *J. Climate*, in press.

Rasch, P. J. and Lawrence, M. 1998. *Recent developments in transport methods at NCAR.* In: MPI-Hamburg report No. 265 (ed. B. Machenhauer), pp. 65–75.

Roelofs, G.-J. and Lelieveld, J. 1995. Distribution and budget of O_3 in the troposphere calculated with a chemistry general circulation model. *J. Geophys. Res.* **100**, 20,983–20,998.

Roelofs, G.-J. and Lelieveld, J. 1997. Model study of the influence of cross-tropopause O3 transports on tropospheric O3 levels. *Tellus* **49B**, 38–55.

Roelofs, G.-J., Lelieveld, J. and Ganzeveld, L. 1998. Simulation of global sulfate distribution and the influence on effective cloud drop radii with a coupled photochemistry-sulfur model. *Tellus* **50B**, 224–242.

Schultz, M., Jacob, D. J., Logan, J. A., Wang, Y., Blake, D. R. 1998. On the origin of tropospheric ozone and NO_x over the tropical South Pacific. *J. Geophys. Res.*, in press.

Thakur, A. N., Singh, H. B., Mariani, P., Chen, Y., Wang, Y., Jacob, D. J., Brasseur, G., Mueller, J.-F. and Lawrence, M. 1998. Distribution of reactive nitrogen species in the remote free troposphere: data and model comparisons. *Atmos. Env.*, in press.

Tie, X. X. and Hess, P. 1997. Ozone mass exchange between the stratosphere and troposphere for background and volcanic sulfate aerosol conditions. *J. Geophys. Res.* **102**, 25,487–25,500.

Wang, Y., Jacob, D. J. and Logan, J. A. 1998. Global simulation of tropospheric O_3–NO_x^--hydrocarbon chemistry (3). Origin of tropospheric ozone and effects of nonmethane hydrocarbons. *J. Geophys. Res.* **103**, 10757–10767.

Yienger, J. J. and Levy, H. II. 1995. Empirical model of global soil-biogenic NO_x emissions. *J. Geophys. Res.* **100**, 11,447–11,464.

Zhang, G. J. and McFarlane, N. A. 1995. Sensitivity of climate simulations to the parameterization of cumulus convection in the Canadian Climate Centre general circulation model. *Atmos. Ocean* **33**, 407–446.